5-25-2022

Virucidal N95 Respirator Face Masks via Ultrathin Surface-Grafted Quaternary Ammonium Polymer Coatings

Mirco Sorci
Rensselaer Polytechnic Institute

Tanner D. Fink
Rensselaer Polytechnic Institute

Vaishali Sharma
Michigan Technological University, vsharma3@mtu.edu

Sneha Singh
Michigan Technological University, snehas@mtu.edu

Ruiwen Chen
Rensselaer Polytechnic Institute

See next page for additional authors

ACS APPLIED MATERIALS & INTERFACES

www.acsami.org

Research Article

Virucidal N95 Respirator Face Masks via Ultrathin Surface-Grafted Quaternary Ammonium Polymer Coatings

Mirco Sorci, Tanner D. Fink, Vaishali Sharma, Sneha Singh, Ruiwen Chen, Brigitte L. Arduini, Katharine Dovidenko, Caryn L. Heldt, Edmund F. Palermo,* and R. Helen Zha*

Cite This: *ACS Appl. Mater. Interfaces* 2022, 14, 25135−25146

Read Online

ACCESS | Metrics & More | Article Recommendations | Supporting Information

ABSTRACT: N95 respirator face masks serve as effective physical barriers against airborne virus transmission, especially in a hospital setting. However, conventional filtration materials, such as nonwoven polypropylene fibers, have no inherent virucidal activity, and thus, the risk of surface contamination increases with wear time. The ability of face masks to protect against infection can be likely improved by incorporating components that deactivate viruses on contact. We present a facile method for covalently attaching antiviral quaternary ammonium polymers to the fiber surfaces of nonwoven polypropylene fabrics that are commonly used as filtration materials in N95 respirators via ultraviolet (UV)-initiated grafting of biocidal agents. Here, C_{12}-quaternized benzophenone is simultaneously polymerized and grafted onto melt-blown or spunbond polypropylene fabric using 254 nm UV light. This grafting method generated ultrathin polymer coatings which imparted a permanent cationic charge without grossly changing fiber morphology or air resistance across the filter. For melt-blown polypropylene, which comprises the active filtration layer of N95 respirator masks, filtration efficiency was negatively impacted from 72.5 to 51.3% for uncoated and coated single-ply samples, respectively. Similarly, directly applying the antiviral polymer to full N95 masks decreased the filtration efficiency from 90.4 to 79.8%. This effect was due to the exposure of melt-blown polypropylene to organic solvents used in the coating process. However, N95-level filtration efficiency could be achieved by wearing coated spunbond polypropylene over an N95 mask or by fabricating N95 masks with coated spunbond as the exterior layer. Coated materials demonstrated broad-spectrum antimicrobial activity against several lipid-enveloped viruses, as well as *Staphylococcus aureus* and *Escherichia coli* bacteria. For example, a 4.3-log reduction in infectious MHV-A59 virus and a 3.3-log reduction in infectious SuHV-1 virus after contact with coated filters were observed, although the level of viral deactivation varied significantly depending on the virus strain and protocol for assaying infectivity.

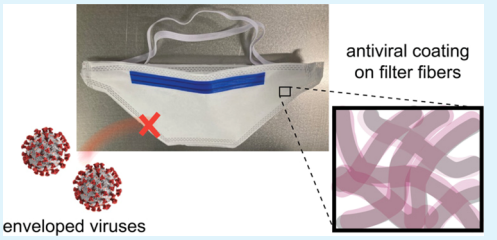

KEYWORDS: *antimicrobial coatings, antiviral filters, quaternary ammonium polymers, face masks, respirator masks*

INTRODUCTION

The past two decades have been marked by multiple outbreaks of severe respiratory illnesses caused by viral infection, including COVID-19, MERS, and SARS. These illnesses are hallmarked by their global spread and high infectivity. According to the National Institute of Allergies and Infectious Diseases, within three months after COVID-19 emerged, nearly 1 million people had been infected and 50,000 people had died.[1] The rapid spread of COVID-19 also led to critical shortages in personal protective equipment (PPE) for healthcare workers, including N95 respirator masks capable of filtering aerosolized virus. These outbreaks have highlighted the importance of face masks as barriers to the transmission of airborne virus. The efficacy of face masks in decreasing disease transmission is not limited to N95, FFP2, or KN95-rated masks (which are capable of filtering out 95% of airborne particles). Studies have shown that even a properly worn fabric covering can significantly arrest the forward motion of aerosol droplets emitted by the wearer while coughing[2] or provide some filtration efficiency.[3] Similarly, the potential role of face masks in improving public health is not restricted to high-profile pandemics, as seasonal influenza causes 12,000−61,000 deaths annually in the U.S.

While masks are an effective barrier to airborne virus transmission, commonly used mask materials are not inherently able to deactivate viruses on contact. As a result, the risk of contamination increases with wear time. Medical PPE is thus intended as single-use items, with regular disposal after each patient exposure, leading to a risk of shortage as well as significant environmental waste. This is particularly problematic for respirator masks, which utilize melt-blown polypropylene (mbPP) with an electret charge as the active filtration layer.[4] Typically made by corona discharge applied

Received: March 7, 2022
Accepted: May 4, 2022
Published: May 25, 2022

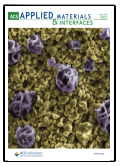

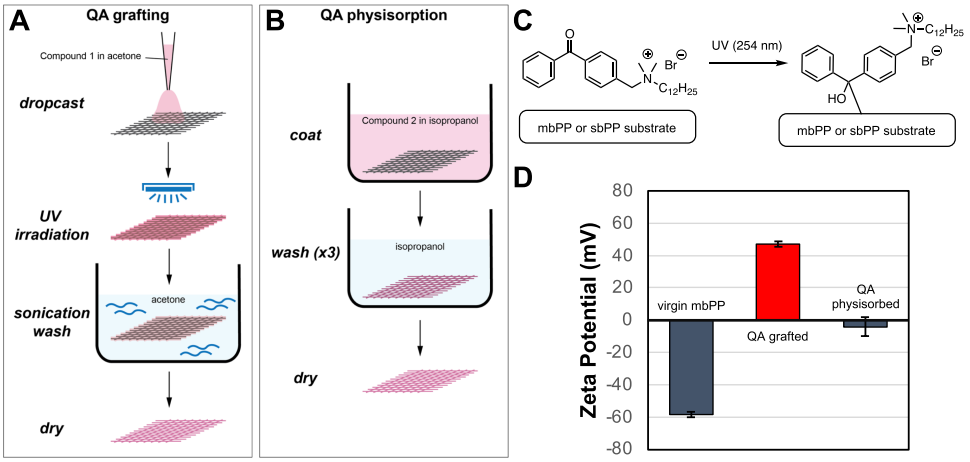

Figure 1. Illustrative protocol of (A) UV-initiated grafting of **QA1** and (B) physisorption of **QA2** to melt-blown polypropylene (mbPP) or spunbond polypropylene (sbPP) filters. (C) Schematic of UV-initiated benzophenone-mediated grafting and cross-linking of Compound **QA1**. (D) Zeta potential of mbPP with and without grafted **QA1** or physisorbed **QA2** as characterized by streaming potential measurements.

during the mbPP fabrication process, this electret charge enhances filtration efficiency without increasing pressure drop across the filter, thus playing a crucial role in maintaining breathability.[4] However, it is also prone to dissipation upon exposure to organic and aqueous solvents, meaning that respirator masks cannot be sterilized for re-use by standard methods such as treating with steam or disinfectant solutions.[5,6]

The ability of face masks to protect against infection can be potentially improved by incorporating components that deactivate viruses on contact without reducing the filtration efficiency. Here, a variety of additives and coatings for application to postfabricated filtration media have been investigated. Of particular interest are metal nanomaterials that can potentially exhibit virucidal behavior. For example, copper exhibits broad-spectrum activity against bacteria and viruses[7−13] and can be incorporated into textile fibers and other polymer products.[14−16] Borkow and colleagues successfully impregnated N95 respirator masks with CuO nanoparticles, demonstrating nearly five-log reduction of infectious human influenza A virus (H1N1) and avian influenza virus (H9N2) without altering the barrier properties of the PPE.[17] More recently, Jung and colleagues showed that a thin copper film deposited onto spunbond polypropylene (sbPP) by vacuum coating can reduce the amount of SARS-CoV-2 by 75% with a minor decrease in filtration efficiency.[18] Similarly, Kumar and colleagues showed that a hybrid coating of shellac/copper nanoparticles sprayed onto nonwoven polypropylene surgical masks can deactivate SARS-CoV-2 virus by photothermal and photocatalytic effects under solar illumination.[19] Aside from copper, other inorganic materials recently investigated for antiviral activity include zinc,[20,21] silver,[22−24] gold,[25,26] graphene,[27−29] and even NaCl.[30] Recent studies have furthermore demonstrated that light-sensitive iron oxide nanoparticles embedded in polymer nanofibers can cause cell membrane permeabilization by photothermal effects.[31] However, one potential concern regarding the use of inorganic materials, which are often applied as nanoparticles noncovalently attached to or embedded in filter fibers, is their adherence tenacity and potential inhaled toxicity in long-term use.

As an alternative to inorganic nanomaterials, immobilization of polycations is a promising approach toward endowing surfaces with antiviral activity. Naturally occurring biopolymers, such as chitosan, are known to have broad spectrum antimicrobial activity.[32] Moreover, the potent antibacterial activity of such amphiphilic polycations by membrane disruption is well-documented.[33,34] Such amphiphilic polycations have also demonstrated the ability to kill lipid-enveloped viruses upon contact.[35−37] For example, Haldar and colleagues showed that branched or linear N,N-dodecyl methyl-polyethylenimines (PEIs) derivatized with hydrophobic groups can yield a 4-log reduction of influenza virus on contact within minutes.[38,39] This virucidal activity was attributed to surface-bound polycations rather than to those leached from the surface. Similarly, amphiphilic polymers and small molecules containing quaternary ammonium salts are well-known biocidal agents that can kill bacteria and enveloped viruses by membrane disruption.[40−42] Recently, Kumaran and colleagues developed a method for dip and spray coating face mask filters with lignin molecules bearing quaternary ammonium functionalities.[43] Here, UV irradiation was used to cross-link the coating and impart structural stability by the addition of photosensitive methacrylates. When applied to mbPP and sbPP filters, the coatings demonstrated up to 5-log inactivation of PR8 influenza virus as well as human alpha and beta coronaviruses. Interestingly, it was found that the coating did not affect the filtration efficiency and pressure drop of sbPP, although mbPP saw a substantial increase in pressure drop after coating, presumably due to occlusion of the small pore structure. Other promising antiviral polymer coatings include N-halamines,[44] amino-modified chitosans,[45] polyphenols,[46] and conjugated polymers.[47]

Considering the antiviral potency of amphiphilic polycations, we have developed a facile approach for covalently attaching quaternized cationic amphiphiles to the fiber surfaces of mbPP and sbPP filtration media. This approach utilizes a UV-active benzophenone moiety to simultaneously polymerize and graft quaternized dimethylaminododecane onto bare polypropylene. The use of benzophenone as a grafting agent is well-suited for modifying filtration media, which are typically made from inert polyolefins such as polypropylene, as its ability to abstract hydrogen atoms from a donor occurs under mild UV light that avoids excessive damage to the polymer substrate.[48] Work by the Locklin group previously showed that antimicrobial cationic polymers with pendant benzophe-

https://doi.org/10.1021/acsami.2c04165
ACS Appl. Mater. Interfaces 2022, 14, 25135−25146

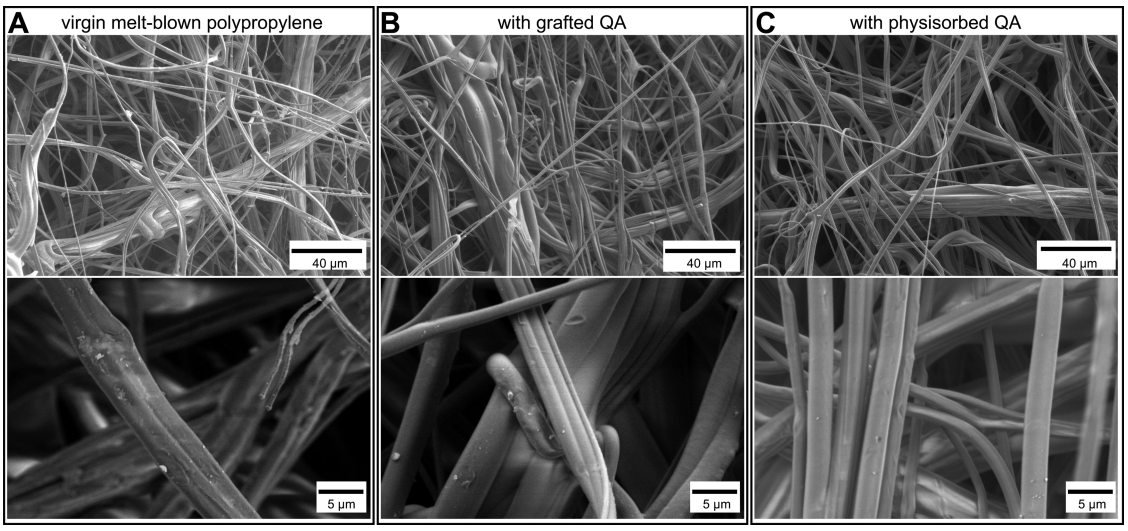

Figure 2. SEM images of (A) uncoated virgin mbPP, (B) mbPP with grafted **QA1**, and (C) mbPP with physisorbed **QA2**. Top row shows low magnification (1000×) while bottom row shows high magnification (5000×) views.

none groups can be readily grafted onto a variety of polymer surfaces, producing ultrathin nonleaching coatings with excellent antibacterial activity,[48] although viral deactivation was not tested. Our work here demonstrates the ability of UV-induced benzophenone grafting chemistry to functionalize mbPP and sbPP with a virucidal quaternary ammonium (QA) coating. Notably, this QA coating does not cause gross changes in the fiber structure nor affect pressure drop across the filter. Furthermore, the QA coating is able to maintain the filtration efficiency of sbPP filters, which when used as the outer protective layer maintains the ability of N95 respirators to meet the National Institute for Occupational Safety and Health (NIOSH) 42 CFR part 84 certification standards for filtration and breathability.[49] We furthermore show that our QA coating exhibits good broad-spectrum on-contact virucidal activity against enveloped viruses as well as gram-negative and gram-positive bacteria. Our coating strategy thus constitutes a viable approach for extending the protection and usage lifespan of respiratory PPE based on polyolefin filtration media.

RESULTS AND DISCUSSION

Application of Cationic Polymers. One challenge in functionalizing filtration media with biocidal molecules containing quaternary ammonium salts is achieving a high density of surface charge without disrupting the fiber structure, which may impact filtration efficiency and air permeability. Generating such dense yet thin and conformal coatings is nontrivial, particularly because some fibers in mbPP (used as N95 filtration media) may be less than 1 μm in diameter. Another challenge for covalently modifying filtration media is the chemical inertness of polypropylene, which does not inherently have reactive groups for derivatization.

We investigated two methods of modifying mbPP and sbPP with QA coatings (Figure 1A,B). First, we covalently grafted **QA1** to fiber surfaces by drop-casting solutions of **QA1** in acetone onto filter swatches, then exposing both sides of the filter swatch to 254 nm UV light to initiate benzophenone cross-linking. Here, the ability of benzophenone to abstract hydrogen atoms from aliphatic C−H groups and form C−C bonds under mild UV irradiation results in simultaneous polymerization and grafting of **QA1** onto the polypropylene surface (Figure 1C). Coated filters are then sonicated in acetone, a good solvent for **QA1**, to remove excess material that did not successfully graft to the surface. It was observed that coated mbPP samples became hydrophilic after QA grafting. Second, to explore more simple methods of coating application that can potentially be applied in an at-home setting by end-users, we investigated simple physisorption of **QA2** to filter surfaces by immersing swatches in a dilute solution of **QA2** dissolved in isopropanol for 15 min, followed by washing with excess isopropanol and drying of the filter swatch in a convection oven.

To confirm successful grafting of QA polymers, we measured the zeta potential of the coated materials using electrokinetic methods for assessing surface charge density (i.e., streaming potential measurements) (Figure 1D). The zeta potential of uncoated mbPP was −58.5 mV, which is consistent with the negative zeta potential of most polyolefins because of preferential adsorption of hydroxyl ions at their surfaces.[50,51] The zeta potential of QA-coated mbPP, whether by grafting or physisorption, was more positive, which is consistent with the deposition of cationic compounds on the surface. For covalently grafted **QA1** on mbPP, a zeta potential of 47.1 mV was measured, showing a complete charge inversion compared to uncoated samples. X-ray photoelectron spectroscopy (XPS) confirmed the successful attachment of **QA1** by an increased Br signal (Figure S6). mbPP samples with physisorbed **QA2** had a zeta potential of −4.2 mV, which is more cationic than uncoated samples but clearly indicates a lower charge density compared to grafted coatings. This result is consistent with the neutralization of attractive electrostatic interactions between the negatively charged surface and the cationic **QA2**, as well as the repulsion of the adsorbed cationic charge to prevent further polyelectrolyte deposition.[52] While overcompensation (i.e., in this case, accumulation of positive surface charge past the point of surface neutrality) is commonly expected for polyelectrolyte adsorption, such an effect is generally facilitated by high polyelectrolyte concentration and molecular weight.[53] Moreover, most polyelectrolyte adsorption studies are performed in aqueous solvents, where liberation of water molecules in a high free energy state at a hydrophobic surface to a lower free energy state in bulk

https://doi.org/10.1021/acsami.2c04165
ACS Appl. Mater. Interfaces 2022, 14, 25135−25146

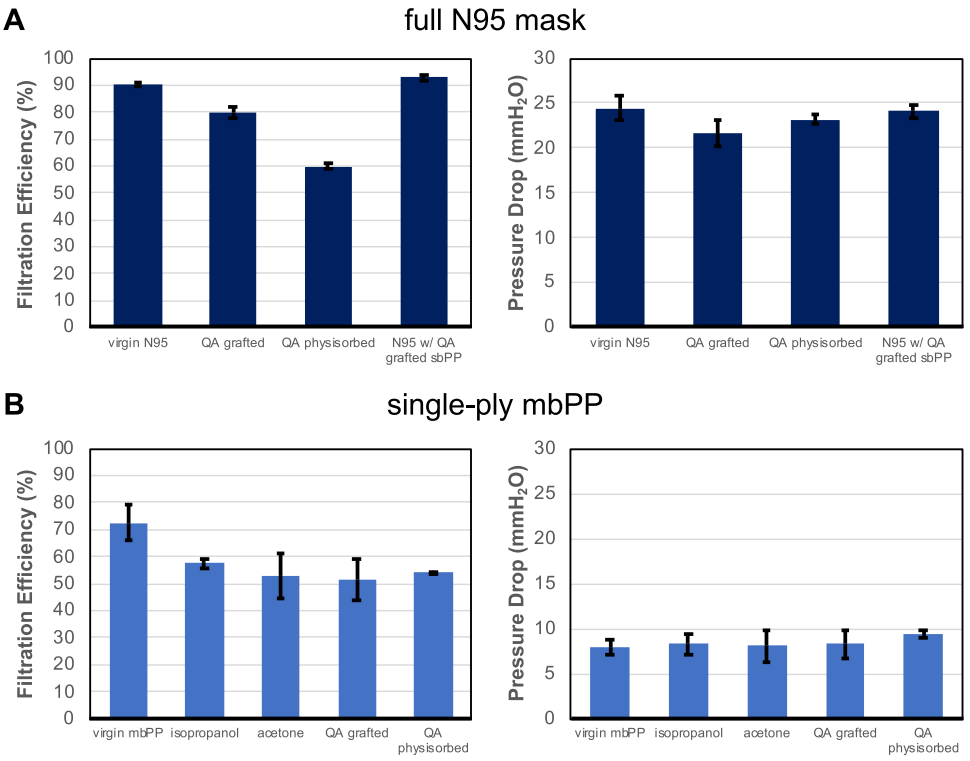

Figure 3. (A) FE and PD across full N95 masks with and without grafted **QA1** or physisorbed **QA2**. FE and PD values are additionally given for uncoated N95 masks layered with a sheet of **QA1**-grafted sbPP. (B) FE and PD results for single-ply N95-grade mbPP with and without grafted **QA1** or physisorbed **QA2**. Results are compared against exposure to acetone and isopropanol without QA. Measurements are performed in triplicate, and error bars represent standard deviations from the mean.

solution provides a thermodynamic driving force.[54] Overcompensation is likely not observed in our physisorbed system because of our low polyelectrolyte concentration and use of isopropanol as a solvent.

Surprisingly, grafting efficiency was lower on sbPP compared to mbPP (Figure S7). The zeta potential of uncoated sbPP was −63.8 mV, which shifted to +37.2 mV after covalent grafting of **QA1**. This positive zeta potential was maintained even after autoclaving, showing stability in aqueous environments and elevated temperatures commonly used for disinfection. However, the zeta potential of **QA1**-grafted sbPP decreased noticeably after exposure to a nonionic surfactant (0.1% Tween 20) or to 70% ethanol (Figure S7), suggesting that a significant amount of **QA1** polymer was not covalently grafted to the fiber surface. Decreased the grafting efficiency on sbPP may be attributed to slight differences in surface chemistry compared to mbPP, which has been treated by corona discharge during manufacturing to generate electret charges. XPS results showing that mbPP has a greater O content than sbPP support this hypothesis (Figure S6). Given these results, further optimization steps, such as pretreatment via exposure to acid or high energy irradiation, are needed to increase the density and stability of grafted QA coatings on sbPP.

The effect of grafted and physisorbed QA coatings coating on mbPP and sbPP filter structures was visualized by scanning electron microscopy (SEM) (Figures 2 and S8). Samples were imaged without sputter coating to better preserve surface morphology. Neither covalent grafting of **QA1** nor physisorption of **QA2** yielded gross observable changes in the fiber diameter or density, although some changes in the surface texture were seen, indicating polymer buildup in some areas.

Filtration Efficiency and Pressure Drop. Various face masks and respirators used as PPE are subject to different regulatory standards depending on their intended application. For example, surgical masks provide a physical barrier to fluids and large particulate materials and must meet specific fluid protection and flammability requirements.[55,56] However, surgical masks are not expected to protect against aerosolized particles, and they are primarily constructed from nonwoven (e.g., spunbond) polypropylene, which does not provide high filtration efficiency (FE). In contrast, air purifying respirators include a layer of electret mbPP that provides high FE. For example, N95 and FFP2 masks must filter at least 95% of airborne particles and provide sufficient breathability under stringent conditions set forth in their certification standards.[49] The need to maintain FE above 95% and acceptable air permeation, as measured by pressure drop (PD) across the filter, presents a particular challenge when chemically modifying filter surfaces. While large particles are blocked by sieving, impaction, and interception mechanisms, the filtration of nanoscale particles substantially smaller than the filter mesh size relies on particle diffusion and adhesion to fiber surfaces. Thus, high FE filtration media typically bear semipermanent electret charges to promote particle adhesion. However, this charge is susceptible to disruption upon solvent exposure.

To characterize the FE and PD of our QA-coated materials against uncoated (NIOSH-certified) materials, we utilized a protocol intended to approximate NIOSH standard procedures for certifying N95 respirator masks. For example, similar preconditioning treatments and NaCl aerosol size distributions, as described in the NIOSH procedure, were used. Some modifications were made to accommodate a smaller sample size and available equipment (Table S1 and Figure S3).

https://doi.org/10.1021/acsami.2c04165
ACS Appl. Mater. Interfaces 2022, 14, 25135−25146

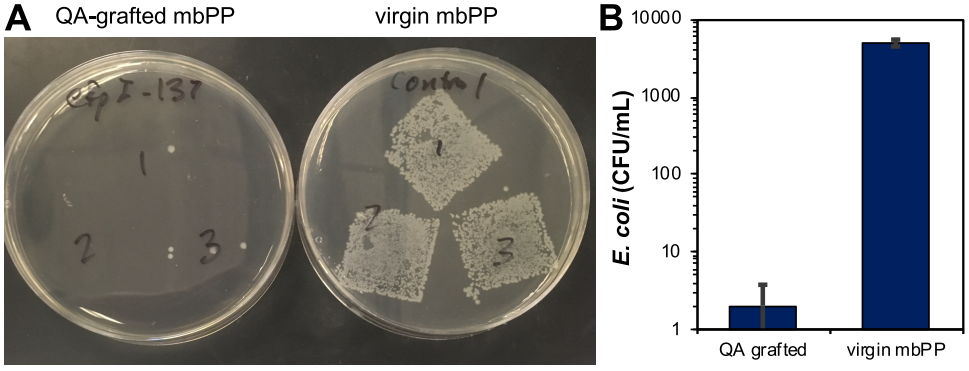

Figure 4. (A) Bacterial growth on culture plates after **QA1**-coated mbPP and virgin mbPP swatches exposed to *E. coli* were pressed against plates. Swatches were eluted prior to contact with plates to qualitatively assess the amount of live bacteria that remained bound after elution. (B) Live *E. coli* eluted from **QA1**-coated mbPP and virgin mbPP swatches as quantified by colony counting.

Specifically, 2.2 cm diameter disks (3.8 cm^2 active filtration area) were used instead of full-size N95 masks (150 cm^2). The aerosol flow rate was adjusted to maintain a similar 9.4 cm/s face velocity as described in the NIOSH procedure. Furthermore, rather than using a photometric detection system, particle detection and counting was performed using a condensation particle counter and differential mobility analyzer, which can resolve FEs for particles as a function of their mobility diameter (Figure S9). These protocol modifications generate results that vary slightly from official NIOSH tests. In our testing conditions, certified N95 filters typically measure between 90−95% FE, although samples with slightly less than 90% FE may also pass NIOSH certification. It should additionally be noted that cycle filtration tests[57] for long-term performance are not required for NIOSH certification and were not performed in our work presented here. However, such investigations would be an important topic for future study.

The FE of a single-ply mbPP layer without a QA coating was measured to be 72.5% +/− 6.5% (Figure 3). In N95 masks, at least two layers of mbPP are typically used to provide sufficient filtration, with the FE of a double layer readily calculated via the following equation:

$$FE_{double} = 1 - (1 - FE_{single})^2$$

Thus, the FE of a double layer of unmodified mbPP is 92.4%, which is consistent with the expected performance of electret mbPP used for N95 applications. The FE of single-ply **QA1**-coated mbPP decreased to 51.3 +/− 7.8%, while the FE of single-ply **QA2**-coated mbPP decreased to 54.2 +/− 0.3%. This FE decrease can be attributed to exposure to organic solvents used in the coating process (acetone for grafting, isopropanol for physisorption), as mbPP exposed to the solvent only showed similar FE. PD across the filters was not significantly changed for coated or solvent exposed materials compared to the virgin mbPP control (Figure 3), indicating that breathability is not negatively impacted. Thus, it is likely that the FE change does not result from fiber structure disruption, a conclusion which is supported by SEM imaging. Rather, solvent exposure likely screens or dissipates the electret charge, which has been shown to significantly impact FE.[5,58] Although our QA polymers are cationic, this permanent polyelectrolyte charge was insufficient to compensate for the loss of electret charge.

FE and DP were also measured for QA coatings applied to full N95 masks, which consist at least two mbPP layers sandwiched between exterior and interior nonwoven polypropylene layers (typically spunbond). Results mirrored those seen with single-ply samples, where both grafted and physisorbed QA showed decreased FE compared to controls (Figure 3). PD also decreased slightly, suggesting possible bundling or aggregation of fibers in one of the layers during coating, although this result does not negatively impact breathability. These results indicate that QA coatings cannot be applied to whole N95 masks as a postfabrication modification. One viable strategy to overcome the impact of coating on the FE of N95 masks is to separately coat sbPP, which is then worn as an additional layer on over an N95 mask. Measurements confirm that this arrangement maintains the FE and PD of N95 masks, indicating no negative impacts of filtration or breathability. Another potent strategy is to utilize coated sbPP as the exterior layer of an N95 mask during fabrication. We obtained an FE of 99.7% for a prototype N95 mask made using **QA1**-grafted sbPP. While this approach cannot be easily implemented by an end user, it can be a value-added step for manufacturers.

Antibacterial Activity. Benzophenones bearing a pendant cationic surfactant have been covalently grafted to polyolefin surfaces, which thereby confers on-contact, nonleaching biocidal activity.[59] The cationic surface is generally thought to electrostatically attract negatively charged cell membrane components, whereas the hydrophobic groups may insert into the nonpolar membrane core, causing membrane disruption and cell death.[60,61] Other plausible antibacterial mechanisms have also been discussed.[62] As a preliminary experiment, we first confirmed that mbPP fibers with grafted **QA1** could indeed exert bactericidal activity (Figure 4). To that end, swatches of **QA1**-grafted mbPP were incubated with a suspension of *E. coli* in MH broth at 37 °C for 2 h, and then, any live cells were eluted with excess buffer. Aliquots were analyzed by streaking onto agar plates and colony counting, which revealed a 3.7-log reduction in the number of viable cells (99.96% killing) relative to the uncoated control (Figures 4B and S10). The swatches were then gently pressed onto agar to transfer any viable live cells remaining bound on the surface (Figure 4A). The coated swatches transferred less than 10, and in some cases zero, *E. coli* colonies to the agar plate, whereas the uncoated control sample transferred a dense, uncountable lawn of colonies that is visually consistent with the finding of >3 log reduction. Similar results were obtained

https://doi.org/10.1021/acsami.2c04165
ACS Appl. Mater. Interfaces 2022, 14, 25135−25146

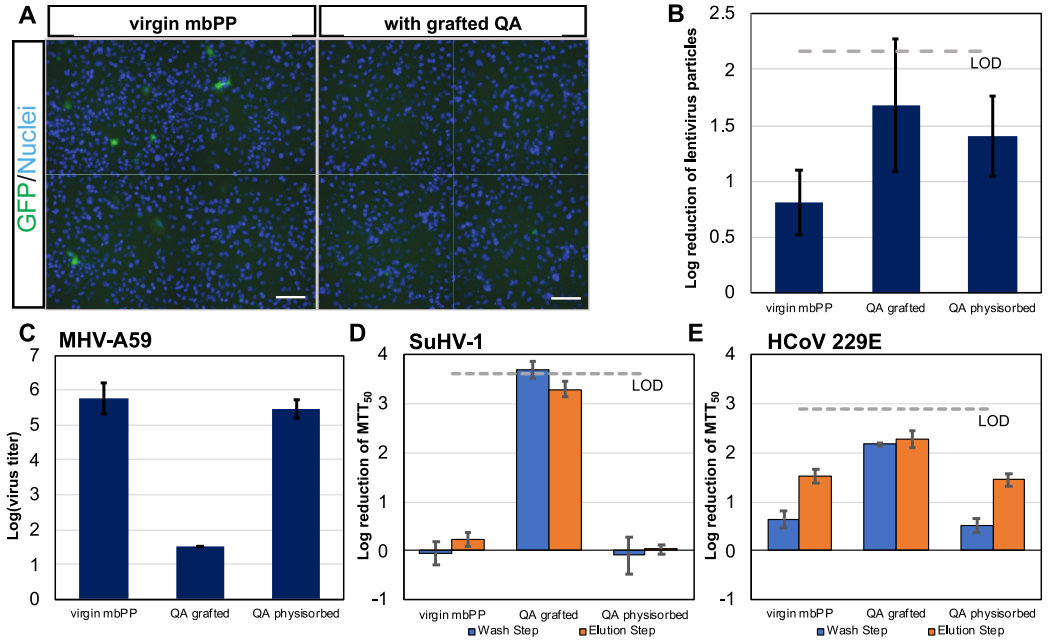

Figure 5. (A) Imaging of host cells infected by fluorescent lentivirus as a method for assessing viral deactivation. (B) Log reduction of infectious lentivirus particles after exposure to mbPP with and without grafted **QA1** or physisorbed **QA2**. Limit of detection (LOD) represents the maximum log reduction detectable because of background GFP fluorescence. (C) Virus titer (per mL) of MHV-A59 virus stocks after exposure to mbPP with and without **QA1** or physisorbed **QA2**. (D) Log reduction of SuHV-1 and (E) HCoV viruses as quantified by an MTT-based assay for host cell metabolic activity. Washing with PBS and elution with 1% BSA are reported separately to provide insight on the extent of viral particle binding to filters.

using gram-positive *S. aureus*, which showed a >2 log reduction in the number of viable cells eluted from **QA1**-grafted mbPP. No viable cells remained bound on **QA1**-grafted mbPP (Figure S11A). Thus, we can conclude that the fabrics exert on-contact broad-spectrum bactericidal activity.

We expect **QA1** to be covalently bound to the mbPP fibers with minimal leaching. We verified this assumption by placing swatches of **QA1**-grafted mbPP onto lawns of *S. aureus* immediately after streaking on nutrient-rich agar plates. After overnight incubation at 37 °C, no zone of inhibition was observed around the **QA1**-grafted mbPP (Figure S11B), indicating that no leaching of the bactericidal quaternary ammonium compound occurred. This finding is consistent with previous literature, confirming the covalent nature of the benzophenone grafting chemistry.[48]

Antiviral Activity. Our primary goal of this work was to study the antiviral activity of QA-coated mbPP fibers, which may differ mechanistically relative to antibacterial activity. Although many examples of cationic and hydrophobic peptides, or synthetic polymers, can be designed to specifically target bacterial membranes selectively over other membrane types, the more intensely hydrophobic cationic surfactants (such as the C_{12}-functionalized QA groups employed in this work) usually exert membrane lysis indiscriminately.[63] Thus, we hypothesized that cationic surfactants would also non-specifically disrupt the integrity of the lipid bilayer on enveloped viruses. The ability of grafted **QA1** and physisorbed **QA2** coatings to deactivate viruses on contact was tested against several model enveloped viruses with biological relevance to those known to cause respiratory illness in humans. We also explored multiple methods for quantifying viral inactivation and infectivity, as various assay techniques reported in the literature can significantly differ in sensitivity and ease of implementation. Additionally, viral inactivation is often sensitive to environmental factors and choice of virus strain. For example, recent studies have found that the efficacy of low-pH viral inactivation depends on the virus strain and the buffering agent used.[64]

First, we examined viral deactivation using a transgenic lentivirus encoding enhanced green fluorescence protein (GFP). Although this lentivirus is nonpathogenic, it serves as a useful model for our infectivity studies, as it was engineered to be a highly infectious vector. Infected cells can be easily identified using fluorescence microscopy. Moreover, the size of this lentivirus (80−100 nm) and its lipid bilayer envelop make it a reasonable approximation for coronaviruses and influenza viruses in our studies. To test the on-contact viral deactivation of QA-coated mbPP compared to bare mbPP, 0.1 mL of lentivirus stock solution was applied to samples, incubated for 1 h, and eluted by gentle agitation. The eluate was then used to infect host cells, the number of infectious virus particles can be simply quantified as the number of GFP-positive host cells (Figure 5A). Results from this assay suggested that both grafted and physisorbed QA coatings exhibit modest virucidal activity, with the grafted coating demonstrating a 1.7-log reduction in infectious virus particles (Figure 5B). A 0.8-log reduction was seen for the uncoated mbPP, which likely indicates some virus remained bound to the filter material even after elution. While this fluorescence-based approach for measuring infectivity is simple to implement and provides quantitative results without user bias in assessing host cell health, a notable disadvantage is the low limit of detection (2.2-log reduction) because of the background fluorescence of uninfected cells. Considering the relatively large standard deviation of the results, it is likely that the virucidal performance of QA-coated materials is underestimated by this assay. Furthermore, because viral stock solutions were not allowed to dry after application to filter samples, some particles

https://doi.org/10.1021/acsami.2c04165
ACS Appl. Mater. Interfaces 2022, 14, 25135−25146

may have remained suspended in solution without contacting the QA coatings, which would also lower the apparent virucidal activity.

Virucidal activity was also assessed using a TCID50 assay, which is a commonly used method to quantify the number of infectious viral units per volume of a solution, also known as a titer. Here, the virus titer is the inverse of the ID50 value, which is the dilution of a virus-containing solution required to infect 50% of a culture based on observing cytopathic effects, divided by the inoculum volume. For this assay, we used MHV-A59 murine hepatitis virus, which is an enveloped mouse coronavirus in the same genus as human coronaviruses such as SARS-CoV and SARS-CoV-2.[65] To maximize the contact of viral particles with the surface of filter fibers, viral stock solutions were deposited in multiple small 2 μL aliquots and allowed to dry before the elution step. This protocol more closely mimics aerosol exposure, which involves droplets with picoliter volumes that are expected to dry rapidly. A 4.3-log reduction in virus titer was seen on mbPP with grafted **QA1** coatings compared to bare mbPP (Figure 5C). Physisorbed **QA2** did not show any virucidal activity, which is consistent with zeta potential results, suggesting that less polymer is deposited on the surface through physisorption. Similar trends in virucidal activity were observed for QA-coated sbPP (Figure S12).

We further assessed the virucidal activity of QA-coated filters using a colorimetric MTT assay for infectivity.[66] Whereas the TCID50 assay is performed by visually inspecting the cytopathic effects of viral infection on host cell morphology, this MTT assay quantitatively measures host cell metabolic activity. Similar to the TCID50 assay protocol, viral stocks were applied to coated and bare mbPP and sbPP in multiple small droplets (5 μL each) and allowed to dry. The samples were then gently washed with a small volume of phosphate buffer to remove unbound virus, and then vortexed vigorously in a larger volume of buffer containing 1% bovine serum albumin (BSA) to elute bound virus. The infectivity of both wash and elution steps were characterized. SuHV-1, a model enveloped virus, and HCoV 229E, a human coronavirus capable of causing respiratory infections in humans, were used in these studies.

For SuHV-1, **QA1**-grafted mbPP samples showed 3.7-log reduction and 3.3-log reduction for the wash and elution steps, respectively (Figure 5D). Here, a high log reduction for the wash step indicates a low viral titer, suggesting that the majority of virus particles bound to the filters as intended. Bare mbPP and mbPP with physisorbed **QA2** showed no virucidal activity. For HCoV 229E, a 2.2-log reduction and 2.3-log reduction were seen for **QA1**-grafted mbPP (Figure 5E). However, bare mbPP and physisorbed **QA2** samples both demonstrated relatively high log reduction values, even in the wash step, which suggest the inability to elute the virus from the filters. The previous literature has also reported this nonspecific binding as a common problem with some enveloped viruses because of their sticky nature,[67] which makes our assessment of virucidal activity using HCoV 229E more challenging. Interestingly, grafted and physisorbed sbPP samples showed minimal reduction of infectious virus particles (Figure S13). This finding is consistent with zeta potential results showing that the application of the QA polymer was less successful on sbPP compared to mbPP. The use of isopropanol to sterilize the filters prior to applying the viral stock likely further removed the QA polymer. This effect was not seen in the TCID50 tests as isopropanol was not used to sterilize the samples before exposure.

CONCLUSIONS

We have shown a simple method for functionalizing melt-blown and spunbond polypropylene filters with on-contact virucidal activity by UV-induced grafting of an amphiphilic quaternary ammonium polymer. This method does not need to be implemented as an added step in the manufacturing process of nonwoven polypropylene as it can be applied postfabrication to existing filter and mask stocks. The UV-grafted coating does not change the fiber structure of filter materials but does endow fiber surfaces with a cationic charge. As a result, coated materials demonstrate bactericidal activity and virucidal activity, likely through a membrane disruption mechanism. Viral deactivation ranges from 1.7-log to 4.3-log reduction values, depending on the assay protocol and the virus strain used. Melt-blown polypropylene was more successfully coated than spunbond polypropylene because of differences in surface chemistry between the two starting materials, and further optimization is needed to produce dense, stable coatings on spunbond filters. Breathability was not impacted by the grafted coating, although the solvents used during the coating process negatively impacted filtration efficiency for N95-rated melt-blown polypropylene. Thus, our grafted coatings should not be applied to whole N95 respirator masks. However, viable alternative strategies, including wearing coated filters over N95 masks or fabricating N95 masks using coated material as an exterior layer, can provide high filtration efficiency and antiviral activity.

METHODS

Materials. *Polymer Synthesis and Coating.* The reagents 4-(bromomethyl)benzophenone (96%), *N*,*N*-dimethyldodecylamine (97%), poly(4-vinyl pyridine) ($M_w \sim 60$ kDa), and 1-bromododecane (97%) were purchased from Millipore Sigma and used as received. Isoamyl alcohol (FG, >98%), acetonitrile (HPLC, >99.8%), and ethanol (anhydrous 200 proof) were purchased from Millipore Sigma and used as received. Isopropyl alcohol (natural >98%) was purchased from Millipore Sigma. Potassium chloride (P9333, BioXtra ≥99.0%) was purchased from Sigma-Aldrich. Sodium hydroxide was purchased from ThermoFisher Scientific. Ultrapure water (resistivity ~18.2 MΩ) was obtained using a WaterPro BT water purification system (Labconco). N95-rated mbPP filtration media was kindly gifted by Hills Incorporated (West Melbourne, FL), and 25 g/m^2 sbPP (WPT P2500D) was kindly gifted by the Advanced Functional Fabrics of America (AFFOA, Cambridge, MA).

Antibacterial Assay. Escherichia coli (ATCC 25922) was purchased as a lyophilized powder from the American Type Culture Collection (ATCC, Manassas, VA). Muller-Hinton (MH) broth, agar, and phosphate buffered saline (PBS) were purchased from Millipore-Sigma.

Lentivirus Deactivation. Human embryonic kidney cells (HEK293T; ATCC CRL-3216) and human lung adenocarcinoma cells (A549; ATTC CCL-185) were purchased from ATCC. Dulbecco's modified Eagle medium (DMEM; Gibco Lot #11995), heat-inactivated fetal bovine serum (HI-FBS; Hyclone Lot #SH0066.03), and penicillin–streptomycin (Gibco Lot #15140) were purchased from Thermo Fisher Scientific. Lentivirus stocks were generated using psPAXS2 (Addgene #12260, gifted by Didier Trono) and pMD2.G (Addgene #12259, gifted by Didier Trono) plasmids purchased from Addgene. Plasmids encoding enhanced green fluorescent protein (pLV-EGFP) were also purchased from Addgene. A Retro-X Concentrator kit was purchased from Clontech 631455 for concentrating viral stocks.

https://doi.org/10.1021/acsami.2c04165
ACS Appl. Mater. Interfaces 2022, 14, 25135−25146

Mouse Coronavirus Deactivation. CCL 9.1 mouse liver cells and murine hepatitis virus (MHV-A59; ATCC V-765) were purchased from ATCC. NCTC 135 media, fibronectin (1 mg/mL solution), fetal bovine serum, and Hanks' balanced salt solution (HBSS) were purchased from Millipore-Sigma.

Human Coronavirus and Suid Herpesvirus Deactivation. Human coronavirus 229E (HCoV 229E, NIH: NR-52726) was obtained from BEI Resources (NIAID). Human lung fibroblast (MRC-5, ATCC CCL-171), Suid herpesvirus 1 strain Aujeszky (SuHV-1, ATCC VR-135), and Vero cells (ATCC CCL-81) were obtained from ATCC. MTT salt (2-(3,5-diphenyltetrazol-2-ium-2-yl)-4,5-dimethyl-1,3 thiazole bromide) was obtained from Alfa Aesar. Cells were grown in Eagle's minimum essential media (EMEM) supplemented with 1% v/v penicillin−streptomycin and 10% v/v FBS at 37 °C with 5% CO_2 and 100% humidity.[68]

Polymer Synthesis and Characterization. *N-(4-Benzoylbenzyl)-N,N-dimethyldodecan-1-aminium bromide (**QA1**).* The C12-quaternized benzophenone **QA1** was prepared in accordance with the literature precedent[59] with minor modifications (Scheme 1). In a 100 mL bomb flask, 4-(bromomethyl)benzophenone (1 g, 3.6 mmol) and *N,N*-dimethyldodecylamine (0.75 g, 3.6 mmol) were dissolved in isoamyl alcohol (10 mL), and a magnetic stir bar was added. The vessel was tightly sealed with a Teflon screw cap equipped with a viton O-ring and heated to 95 °C in an aluminum heating block, upon which the turbid suspension became optically clear. After stirring for 24 h, the vessel was cooled to room temperature, and the solution was concentrated under reduced pressure to a yellow, viscous oil that slowly solidified to a waxy solid upon standing at −20 °C for 1 h. The waxy solid was dissolved in a minimum amount of methylene chloride (~1 mL) and recrystallized by slow addition of a hexane/ethyl acetate mixture (2:1 v/v). Solids were obtained by vacuum filtration and washed with excess cold hexanes. Upon drying in vacuo for 18 h, the pure product was obtained as a white solid (1.6 g, 88% yield). The ^{1}H NMR spectra (Figure S1) is in accordance with the literature.[59]

Scheme 1. Synthesis of Compound QA1

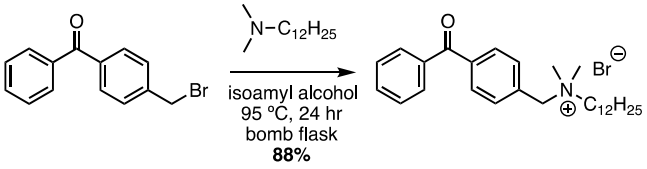

*Poly(1-dodecyl-4-vinyl pyridinium bromide) (**QA2**).* Compound **QA2** was prepared according to the literature precedent[69] with minor modifications (Scheme 2). The polymer poly(4-vinyl pyridine), M_n = (1.3 g, 12.3 mmol pyridine units) and 1-bromododecane (3.6 mL, 14.8 mmol) were dissolved in acetonitrile (5 mL) and ethanol (2 mL) in a 25 mL round bottom glass flask equipped with a magnetic stir bar and attached to a cold water reflux condenser. The clear yellow solution was heated to reflux for 96 h. Upon cooling to room temperature, the solution was concentrated under reduced pressure to yield a viscous brown oil that solidified upon standing. The crude material was dissolved in hot ethanol (5 mL) and precipitated by dropwise addition into cold acetone (20 mL) with rapid stirring. The precipitate was collected by centrifugation, and the process was repeated twice to obtain a white powder (3.0 g, 63% yield). The ^{1}H NMR spectra (Figure S2) result is in accordance with the literature.[69]

Scheme 2. Synthesis of Compound QA2

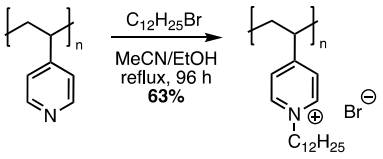

Covalent Grafting to Filtration Media. Compound **QA1** was dissolved in acetone (10 mg/mL), and an aliquot (150 μL) was drop-cast onto each swatch (25 × 25 mm^2) of mbPP. After solvent evaporation, swatches were irradiated under a UV lamp (6 W, 254 nm) for 10 min per side (Figure 1). Swatches were then sonicated in excess acetone for 10 min to remove unbound material from the fiber surfaces and dried under vacuum for 1 h. The same procedure was followed for sbPP substrates.

Physisorption to Filtration Media. Compound **QA2** was dissolved at 1 mg/mL in isopropanol, and mbPP and sbPP substrates were fully immersed in the solution for 15 min at room temperature on a 60 rpm orbital shaker. The substrates were then washed by dipping in three sequential baths containing clean isopropanol for at least 30 s each and dried in a convection oven at 70 °C for 1 h.

Zeta Potential Measurement. Surface zeta potential of coated and uncoated filters was measured using a commercial electrokinetic analyzer (SurPASS3, Anton Paar GmbH, Austria). Two 20 × 10 mm^2 swatches were cut and fixed onto both sides of the rectangular planar sample holders of a SurPASS adjustable gap cell using double-sided polyester tape (#4965, Tesa Tape Inc., Charlotte, NC). Before each measurement, the samples were rinsed three times with the working electrolyte solution. For each coating, three streaming voltage measurements were collected, followed by three streaming current measurements. All measurements were performed at 22 °C. The gap distance was kept constant and equal to ~100 μm. The electrolyte solution was prepared by dissolving KCl (10 mM) in ultrapure water, and the pH was kept at ~7.4 using 50 mM NaOH.

X-ray Photoelectron Spectroscopy. Samples were cut with standard scissors to approximately 2 × 5 mm^2 and mounted under a Mo mask on a 1-inch PHI sample holder. The system was pumped to a base vacuum pressure of approximately 5 × 10^{-7} Torr. The PHI neutralizer system was also used, bringing the base pressure to approximately 3 × 10^{-6} Torr due to the Ar ion gun. For measurement, a beam of 100 μm diameter with 25 W power was rastered over an area of 500 × 500 $μm^2$.

Scanning Electron Microscopy. SEM was used to study the effect of coatings on the fiber surface morphology. Samples were prepared by cutting a small (approximately 5 × 4 mm^2) section of coated and uncoated mbPP and sbPP using scissors, and then mounting the cut section on double-sided carbon conducting tape placed over Al stubs. All tools for cutting and handling were cleaned with isopropanol prior to each use. During imaging, areas at the sample edges as well as the areas where the material was handled with tweezers were avoided. Samples were imaged without sputter-coating to ensure accurate assessment of fiber surfaces. A field emission SEM (Versa 3D Focused Ion Beam-SEM, Thermo Fisher Scientific) was used for imaging. The images were collected in low-vacuum mode to facilitate imaging of uncoated samples, with partial pressure in the range of 140−160 Pa. Low accelerating voltage (2 kV) and 4.5−5 mm sample working distance were used. Images were obtained using a low-vacuum secondary electron detector (LVSED).

FE and PD Testing. The FE and PD testing procedure used approximates NIOSH Procedure No. TEB-APRSTP-0059 rev. 3.2 "Determination of Particulate Filter Efficiency Level for N95 Series Filters Against Solid Particulates for Non-Powered, Air-Purifying Respirators Standard Testing Procedure (STP)", which meets the minimum certification standards set forth in 42 CFR, Part 84, Subpart K, §84.181 "Non-Powered Air-Purifying Particulate Respirators" and to NIOSH Procedure No. TEB-APR-STP-0007 rev. 2.3 "Determination of Inhalation Resistance Test, Air-Purifying Respirators Standard Testing Procedure (STP)", which meets the minimum inhalation resistance requirements of 42 CFR, Part 84, Subpart K, §84.180 "Airflow resistance tests". Significant modifications (Table S1) to these NIOSH procedures were made to accommodate equipment configuration (Figure S3) and are described as follows: samples were cut to 2.2 cm diameter discs (active area is 3.8 cm^2) and were preconditioned at 38 °C with 85 ± 5% relative humidity for at least 20 h. FE was tested using a neutralized, Boltzmann equilibrated NaCl aerosol with 75 ± 20 nm particle size (count median diameter) at a concentration of approximately 10 mg/m^3 and a flow rate of

https://doi.org/10.1021/acsami.2c04165
ACS Appl. Mater. Interfaces 2022, 14, 25135−25146

approximately 2.0 L per minute (9.6 cm/s equivalent face velocity). Testing was performed at approximately 22 °C and 11% relative humidity for 15 min. Particles were sized and counted using a differential mobility analyzer (TSI 3081) and condensation particle counter (TSI 3775), respectively. A schematic of the full setup is presented in Figure S3. Conditions varied slightly between samples and are individually summarized in Table S2. Triplicates of each sample were measured.

Fabrication and Testing of N95 Mask with a Coated Material. N95-style respirator masks were fabricated using coated material for FE testing. Here, sbPP with UV-grafted **QA1** was stacked as the outermost layer (furthest away from the mask wearer), with an unmodified mbPP filtration layer in the middle and another unmodified sbPP as the innermost layer (against the skin of the mask wearer). These three layers were laser cut and ultrasonically welded together, and elastic straps and an adhesive nose bridge were added to form the final mask (Figure S4). FE of this constructed mask was measured exactly following NIOSH Procedure No. TEB-APR-STP-0059 Rev. 3.2 using a TSI Model 8130A Automated Filter Tester.

Antibacterial Assay. The on-contact antibacterial activity of coated filtration media was investigated using the colony-counting method on nutrient-rich agar. First, swatches (25 × 25 mm^2) of mbPP, with and without a UV-grafted coating of **QA1**, were sterilized with 70% ethanol (200 μL) for 10 min, followed by washing with sterile deionized water (3 × 200 mL), to yield prewetted starting swatches. It should be noted that dried mbPP swatches are hydrophobic, whereas prewetted swatches readily absorb assay media. The prewetted mbPP, both coated with **QA1** and uncoated controls, were inoculated with an aliquot (100 μL) of ∼5 × 10^6 CFU/mL *E. coli* stock in PBS for 2 h at 37 °C. After the incubation time, PBS (0.8 mL) was added and incubated for 10 min with orbital shaking to elute out any live bacteria. Then, serial 10-fold dilutions were streaked onto MH agar plates for colony counting (using a 20 μL aliquot from each of the 10×, 100×, and 1000× dilutions). To quantify live bacteria remaining on the filters after elution, the wet swatches were then placed directly onto agar plates with no dilution, incubated for 10 min, and then removed. All agar plates were incubated at 37 °C overnight. The log reduction in viable *E. coli*, relative to the uncoated control, was calculated from colony counting on the agar plates. Coated and uncoated samples were measured in triplicate. The same procedure was followed using *Staphylococcus aureas*, a gram-positive bacteria, except that the cell concentration applied was 5 × 10^5 CFU/mL.

Nonleaching Assay. A lawn of *S. aureus* was streaked onto nutrient-rich agar plates at ∼10^6 CFU, and a swatch of **QA1**-coated mbPP was placed immediately on top of the lawn. The plate was incubated overnight at 37 °C, and optical imaging was used to examine the margins of the mbPP swatch for a zone of inhibition.

Fluorescent Lentivirus Deactivation. HEK293T human embryonic kidney cells and A549 human lung adenocarcinoma cells were maintained at 37 °C with 5% CO_2 in DMEM supplemented with 10% HI-FBS and 100 U/mL penicillin−streptomycin. Lentivirus stocks were generated by transfecting HEK293T cells with second-generation LV plasmids encoding enhanced green fluorescent protein (pLV-EGFP), followed by collecting and concentrating the lentivirus 48 and 72 h post-transfection. Lentivirus stocks were concentrated with a Retro-X Concentrator kit (Clontech 631455), aliquoted for single use, and stored at −80 °C until further use.

Coated and uncoated samples were cut to 25 × 25 mm^2 square swatches, sterilized by immersing in 70% isopropanol for 5 min, and rinsed with tissue culture grade deionized water immediately prior to performing deactivation assays. In order to maintain wettability, the swatches were kept immersed in water and not allowed to dry out before exposure to lentivirus solutions. Active lentivirus stocks were diluted to 2 × 10^7 virus particles per mL in DMEM, and 0.1 mL of this working solution was spiked directly onto each sample swatch. Samples were incubated protected from light at room temperature for 1 h. Then, virus particles were eluted by adding 1.5 mL of DMEM supplemented with 1.5% HI-FBS and gently shaking for 15 min. A 10-fold dilution series was made using each eluate solution, and 60 μL of each dilution was transferred, in duplicate, to A549 cells cultured to confluency in 96-well plates. The plates were incubated at 37 °C, 5% CO_2 for 48 h before fixing with 4% paraformaldehyde, treated with 4,6′ diamidino-2-phenylindole (DAPI) nuclear stain for 15 min, and imaged with a ThermoScientific Cellomics ArrayScan XTI high-content fluorescent microscope. Biological triplicates were performed for each coating type, as well as for the uncoated control. The number of infectious virus particles recovered per sample was calculated by overlaying the DAPI and GFP channels and counting the number of cells (based on DAPI staining) associated with a GFP signal using the ArrayScan software. Uninfected host cells were similarly imaged to determine the level of background GFP signals, which was considered the LOD for this assay. As a positive control to assess lentivirus stability, working lentivirus solution was incubated without exposure to coated or uncoated samples before infecting host cells. To avoid confounding results due to the infection of a host cell by multiple viral particles, the number of infectious particles was calculated using the eluate dilution that provided closest to but not more than 40% GFP-positive cells. Log reduction values (LRV) for samples exposed to uncoated material, grafted, and physisorbed QA compared to positive controls were calculated as follows:

$$\mathrm{LRV} = \log_{10}\left(\frac{\text{infections virus particles}_{\text{no exposure}}}{\text{infections virus particles}_{\text{with exposure}}}\right) \quad (1)$$

Mouse Coronavirus Deactivation. MHV-A59 virus and CCL 9.1 mouse liver host cells were used to quantify viral deactivation by a standard tissue culture infectious dose (TCID50) endpoint assay. CCL 9.1 cells were cultured in cell growth medium (CGM) containing NCTC 135 supplemented with 10% FBS. In preparation for assays, 96-well plates were coated with fibronectin by dispensing 100 μL of 2 μg/mL fibronectin in HBSS into each well. Plates were incubated for 1 h at 37 °C before aspirating away excess fibronectin solution. CCL 9.1 cells were then plated at a density of 2.2 × 10^4 cells/well for 24 h at 37 °C, 5% CO_2 until confluent.

For TCID50 testing, MHV-A59 virus was suspended in virus assay medium (VAM) containing NCTC135 with 2% FBS at 2 × 10^3 PFU/mL. Coated and uncoated mbPP and sbPP samples were cut to 1.5 × 1.5 cm^2 square swatches and placed on a Petri dish. Then, 10 droplets of 2 μL of MHV-A59 virus stock were spotted onto each swatch. The swatches were allowed to dry in the biosafety cabinet for 1 h before eluting with VAM. For elution, hydrophilic samples (substrates grafted with Compound **QA1**) were placed into a 5 μm centrifugal filter unit with 500 μL of VAM, vortexed, and centrifuged at 2000 g for 1 min at 4 °C. Hydrophobic samples (uncoated substrates and substrates with physisorbed Compound **QA2**) were directly washed with 500 μL of VAM. A 10-fold dilution series was made using each eluted viral extract. To infect CCL 9.1 cells, the CGM media from each well was replaced by 100 μL of each diluted viral extract following the plate layout in Figure S3. For no-virus controls, sample swatches were exposed to VAM only following the same protocol. For positive controls, VAM with 1% Triton X-100 was added to CCL 9.1 cells. The plates were then placed in a 37 °C, 5% CO_2 incubator for 40 h. Virus-induced cytopathic activity was evaluated as present (+) or not present (−) by observing cell morphology under a microscope. Each coating was characterized in triplicate. ID50 values, defined as the dilution of a virus required to infect 50% of test units inoculated, was calculated from the assay using the Reed−Muench method.[70] The virus titer in terms of infectious viral units per volume was calculated as the inverse of the ID50 divided by the volume of the viral inoculum (0.1 mL). It should be noted that this testing was not performed for certification purposes.

Human Coronavirus and Suid Herpesvirus Deactivation. Human coronavirus 229E (HCoV 229E was propagated and titrated on MRC-5 human lung fibroblast cells. Suid herpesvirus 1 strain Aujeszky (SuHV-1) was propagated and titrated on CCL-81 Vero cells. Following previously published protocols,[68] crude virus was clarified by centrifugation and stored at −80 °C until used.

https://doi.org/10.1021/acsami.2c04165
ACS Appl. Mater. Interfaces 2022, 14, 25135−25146

Coated and uncoated samples were cut into 1 × 1 cm^2 swatches using a sterilized blade. Each sample swatch was sterilized with about 20 μL of 70% ethanol. After 10 min, the samples were washed twice by immersing each swatch in 30 mL of PBS (pH 7.2) for 30 min with gentle horizontal rocking on. Each swatch was carefully placed into one well of a 24-well plate and spotted with 10 droplets of 5 μL of crude virus stock,[71] prepared as described previously.[68] Swatches were incubated at room temperature in the biosafety cabinet for 2.5 h or until dry. Each swatch was then gently washed with 200 μL of 20 mM phosphate buffer at pH 7.0 with horizontal rocking for 30 min. The wash buffer was collected from the well and titrated as described below to assess the infectivity of virus removed by this wash step. Each swatch was then placed in a 15 mL conical tube with 1.3 mL of elution buffer containing completed media plus 1% bovine serum albumin (BSA). The tube was vortexed for 1.5 min and then centrifuged at 1500 rpm for 3 min in a ThermoScientific Sorvall ST16R Centrifuge. The infectivity of the resulting supernatant, denoted "eluant", was measured with a cell viability assay using MTT.

Infectivity was measured by diluting wash and eluant solutions taken from swatches 1:5 serially across a row in a 96-well plate. After six days, MTT salt (2-(3,5-diphenyltetrazol-2-ium-2-yl)-4,5-dimethyl-1,3 thiazole bromide) was added to each well for 4 h and then solubilized with 10% sodium dodecyl sulfate at a pH of 2. The absorbance of each well was read at a wavelength of 550 nm with a BioTek Synergy Mx microplate reader to determine the 50% infectious dose, reported as MTT_{50}/mL.[66] Final viral concentrations were reported as the log reduction value (LRV) compared to viral stocks unexposed to filter samples, defined in eq 2:

$$\mathrm{LRV} = \log_{10}\left(\frac{\mathrm{MTT}_{50,\text{no exposure}}}{\mathrm{MTT}_{50,\text{with exposure}}}\right) \quad (2)$$

■ ASSOCIATED CONTENT

Supporting Information

The Supporting Information is available free of charge at https://pubs.acs.org/doi/10.1021/acsami.2c04165.

Additional information regarding protocols used in the filtration efficiency and pressure drop measurements, SEM images and zeta potential measurements of spunbond materials, XPS results, and virucidal activity on spunbond materials (PDF)

■ AUTHOR INFORMATION

Corresponding Authors

Edmund F. Palermo − *Department of Materials Science and Engineering, Rensselaer Polytechnic Institute, Troy, New York 12180, United States;* orcid.org/0000-0003-3656-787X; Email: palere@rpi.edu

R. Helen Zha − *Department of Chemical and Biological Engineering and Center for Biotechnology and Interdisciplinary Studies, Rensselaer Polytechnic Institute, Troy, New York 12180, United States;* orcid.org/0000-0002-0766-5705; Email: zhar@rpi.edu

Authors

Mirco Sorci − *Department of Chemical and Biological Engineering and Center for Biotechnology and Interdisciplinary Studies, Rensselaer Polytechnic Institute, Troy, New York 12180, United States;* orcid.org/0000-0001-6053-6702

Tanner D. Fink − *Department of Chemical and Biological Engineering and Center for Biotechnology and Interdisciplinary Studies, Rensselaer Polytechnic Institute, Troy, New York 12180, United States*

Vaishali Sharma − *Department of Biological Sciences and Health Research Institute, Michigan Technological University, Houghton, Michigan 49931, United States;* orcid.org/0000-0003-4069-314X

Sneha Singh − *Health Research Institute and Department of Chemical Engineering, Michigan Technological University, Houghton, Michigan 49931, United States*

Ruiwen Chen − *Department of Materials Science and Engineering, Rensselaer Polytechnic Institute, Troy, New York 12180, United States*

Brigitte L. Arduini − *Center for Biotechnology and Interdisciplinary Studies, Rensselaer Polytechnic Institute, Troy, New York 12180, United States*

Katharine Dovidenko − *Center for Materials, Devices, and Integrated Systems, Rensselaer Polytechnic Institute, Troy, New York 12180, United States*

Caryn L. Heldt − *Health Research Institute and Department of Chemical Engineering, Michigan Technological University, Houghton, Michigan 49931, United States;* orcid.org/0000-0002-0776-8763

Complete contact information is available at: https://pubs.acs.org/10.1021/acsami.2c04165

Notes

The authors declare no competing financial interest.

■ ACKNOWLEDGMENTS

The authors acknowledge Timothy Robson and Hills Inc. for generously providing N95-grade melt-blown polypropylene; Dr. Greg Rutledge, Dr. Jeonyoon Lee, and Dr. Junli Hao at MIT for performing filtration efficiency and pressure drop experiments on filter samples as part of the Advanced Functional Fabrics of America, Inc. (AFFOA) partnership; Kristen Mulherin at AFFOA for providing spunbond polypropylene and prototyping N95 masks; and Patrick Casey and Cheryl Gomes at the University of Massachusetts Lowell for performing filtration efficiency testing on prototyped N95 masks as part of the AFFOA partnership. The authors acknowledge Lalitha Parameswaran at MIT Lincoln Laboratory for performing TCID50 testing with funding from AFFOA. Work supported by AFFOA and also includes support from U.S. Army ARDEC under Agreement number W15QKN-16-3-0001. The authors also acknowledge Michigan Tech College of Engineering for funding MTT infectivity assays, including collaborator Dr. Bruce Lee and NSF #CBET-1818906 (C.L.H.), and also thank BEI for providing the original HCoV 229E virus stock. All other work was supported by NSF #CBET-2028763, including funding for R.H.Z., E.F.P., M.S., and T.D.F.

■ REFERENCES

(1) *National Institute of Allergy and Infectious Diseases*. Covid-19, MERS & SARS, 2021, https://www.niaid.nih.gov/diseases-conditions/covid-19. Accessed 20 January, 2022.

(2) Verma, S.; Dhanak, M.; Frankenfield, J. Visualizing the Effectiveness of Face Masks in Obstructing Respiratory Jets. *Phys. Fluids* **2020**, *32*, No. 061708.

(3) Konda, A.; Prakash, A.; Moss, G. A.; Schmoldt, M.; Grant, G. D.; Guha, S. Aerosol Filtration Efficiency of Common Fabrics Used in Respiratory Cloth Masks. *ACS Nano* **2020**, *14*, 6339−6347.

(4) Kravtsov, A.; Brünig, H.; Zhandarov, S.; Beyreuther, R. The Electret Effect in Polypropylene Fibers Treated in a Corona Discharge. *Adv. Polym. Technol.* **2000**, *19*, 312−316.

(5) Liao, L.; Xiao, W.; Zhao, M.; Yu, X.; Wang, H.; Wang, Q.; Chu, S.; Cui, Y. Can N95 Respirators Be Reused After Disinfection? How Many Times? *ACS Nano* **2020**, *14*, 6348−6356.
(6) Smith, J. S.; Hanseler, H.; Welle, J.; Rattray, R.; Campbell, M.; Brotherton, T.; Moudgil, T.; Pack, T. F.; Wegmann, K.; Jensen, S.; Jin, J.; Bifulco, C. B.; Prahl, S. A.; Fox, B. A.; Stucky, N. L. Effect of Various Decontamination Procedures on Disposable N95 Mask Integrity And SARS-Cov-2 Infectivity. *J. Clin. Transl. Sci.* **2020**, *5*, No. e10.
(7) Govind, V.; Bharadwaj, S.; Sai Ganesh, M. R.; Vishnu, J.; Shankar, K. V.; Shankar, B.; Rajesh, R. Antiviral Properties of Copper and Its Alloys to Inactivate Covid-19 Virus: A Review. *BioMetals* **2021**, *34*, 1217−1235.
(8) Vincent, M.; Duval, R. E.; Hartemann, P.; Engels-Deutsch, M. Contact Killing and Antimicrobial Properties of Copper. *J. Appl. Microbiol.* **2018**, *124*, 1032−1046.
(9) Cortes, A.; Zuñiga, J. M. Use of Copper to Help Prevent The Transmission Of SARS-Coronavirus and Influenza Viruses. A General Review. *Diagn. Microbiol. Infect. Dis.* **2020**, *98*, No. 115176.
(10) van Doremalen, N.; Bushmaker, T.; Morris, D. H.; Holbrook, M. G.; Gamble, A.; Williamson, B. N.; Tamin, A.; Harcourt, J. L.; Thornburg, N. J.; Gerber, S. I.; Lloyd-Smith, J. O.; de Wit, E.; Munster, V. J. Aerosol and Surface Stability of SARS-Cov-2 as Compared with SARS-CoV-1. *N. Engl. J. Med.* **2020**, *382*, 1564−1567.
(11) Behzadinasab, S.; Chin, A.; Hosseini, M.; Poon, L.; Ducker, W. A. A Surface Coating that Rapidly Inactivates SARS-CoV-2. *ACS Appl. Mater. Interfaces* **2020**, *12*, 34723−34727.
(12) Hosseini, M.; Chin, A. W. H.; Behzadinasab, S.; Poon, L. L. M.; Ducker, W. A. Cupric Oxide Coating that Rapidly Reduces Infection by SARS-Cov-2 via Solids. *ACS Appl. Mater. Interfaces* **2021**, *13*, 5919−5928.
(13) Sousa, B. C.; Cote, D. L. Antimicrobial Copper Cold Spray Coatings and SARS-CoV-2 Surface Inactivation. *MRS Adv.* **2020**, *5*, 2873−2880.
(14) Gabbay, J.; Borkow, G.; Mishal, J.; Magen, E.; Zatcoff, R.; Shemer-Avni, Y. Copper oxide Impregnated Textiles with Potent Biocidal Activities. *J. Ind. Text.* **2006**, *35*, 323−335.
(15) Borkow, G.; Gabbay, J. Putting Copper into Action: Copper-Impregnated Products with Potent Biocidal Activities. *FASEB J.* **2004**, *18*, 1728−1730.
(16) Borkow, G.; Sidwell, R. W.; Smee, D. F.; Barnard, D. L.; Morrey, J. D.; Lara-Villegas, H. H.; Shemer-Avni, Y.; Gabbay, J. Neutralizing Viruses in Suspensions by Copper Oxide-Based Filters. *Antimicrob. Agents Chemother.* **2007**, *51*, 2605−2607.
(17) Borkow, G.; Zhou, S. S.; Page, T.; Gabbay, J. A Novel Anti-Influenza Copper Oxide Containing Respiratory Face Mask. *PLoS One* **2010**, *5*, No. e11295.
(18) Jung, S.; Yang, J.-Y.; Byeon, E.-Y.; Kim, D.-G.; Lee, D.-G.; Ryoo, S.; Lee, S.; Shin, C.-W.; Jang, H. W.; Kim, H. J.; Lee, S. Copper-Coated Polypropylene Filter Face Mask with SARS-Cov-2 Antiviral Ability. *Polymer* **2021**, *13*, 1367.
(19) Kumar, S.; Karmacharya, M.; Joshi, S. R.; Gulenko, O.; Park, J.; Kim, G.-H.; Cho, Y.-K. Photoactive Antiviral Face Mask with Self-Sterilization and Reusability. *Nano Lett.* **2021**, *21*, 337−343.
(20) El-Megharbel, S. M.; Alsawat, M.; Al-Salmi, F. A.; Hamza, R. Z. Utilizing of (Zinc Oxide Nano-Spray) for Disinfection Against "SARS-Cov-2" and Testing its Biological Effectiveness on Some Biochemical Parameters During (COVID-19 Pandemic)—"ZnO Nanoparticles Have Antiviral Activity against (SARS-CoV-2)". *Coatings* **2021**, *11*, 1114.
(21) Kumar, A.; Sharma, A.; Chen, Y.; Jones, M. M.; Vanyo, S. T.; Li, C.; Visser, M. B.; Mahajan, S. D.; Sharma, R. K.; Swihart, M. T. Copper@ZIF-8 Core-Shell Nanowires for Reusable Antimicrobial Face Masks. *Adv. Funct. Mater.* **2021**, *31*, No. 2008054.
(22) Li, Y.; Leung, P.; Yao, L.; Song, Q. W.; Newton, E. Antimicrobial Effect of Surgical Masks Coated with Nanoparticles. *J. Hosp. Infect.* **2006**, *62*, 58−63.
(23) Wang, H.; Wang, J.; Hong, J.; Wei, Q.; Gao, W.; Zhu, Z. Preparation and Characterization of Silver Nanocomposite Textile. *J. Coat. Technol. Res.* **2007**, *4*, 101−106.
(24) Salleh, A.; Naomi, R.; Utami, N. D.; Mohammad, A. W.; Mahmoudi, E.; Mustafa, N.; Fauzi, M. B. The Potential of Silver Nanoparticles for Antiviral and Antibacterial Applications: A Mechanism of Action. *Nanomaterials* **2020**, *10*, 1566.
(25) Meléndez-Villanueva, M. A.; Morán-Santibañez, K.; Martínez-Sanmiguel, J. J.; Rangel-López, R.; Garza-Navarro, M. A.; Rodríguez-Padilla, C.; Zarate-Triviño, D. G.; Trejo-Ávila, L. M. Virucidal Activity of Gold Nanoparticles Synthesized by Green Chemistry Using Garlic Extract. *Viruses* **2019**, *11*, 1111.
(26) Papp, I.; Sieben, C.; Ludwig, K.; Roskamp, M.; Böttcher, C.; Schlecht, S.; Herrmann, A.; Haag, R. Inhibition of Influenza Virus Infection by Multivalent Sialic-Acid-Functionalized Gold Nanoparticles. *Small* **2010**, *6*, 2900−2906.
(27) Zhong, H.; Zhu, Z.; Lin, J.; Cheung, C. F.; Lu, V. L.; Yan, F.; Chan, C.-Y.; Li, G. Reusable and Recyclable Graphene Masks with Outstanding Superhydrophobic and Photothermal Performances. *ACS Nano* **2020**, *14*, 6213−6221.
(28) Huang, L.; Xu, S.; Wang, Z.; Xue, K.; Su, J.; Song, Y.; Chen, S.; Zhu, C.; Tang, B. Z.; Ye, R. Self-Reporting and Photothermally Enhanced Rapid Bacterial Killing on a Laser-Induced Graphene Mask. *ACS Nano* **2020**, *14*, 12045−12053.
(29) Maqbool, I.; Rehman, F.; Soomro, F.; Bhatti, Z.; Ali, U.; Jatoi, A. H.; Lal, B.; Iqbal, M.; Phulpoto, S.; Ali, A.; Thebo, K. H. Graphene-Based Materials for Fighting Coronavirus Disease 2019: Challenges and Opportunities. *ChemBioEng Rev.* **2021**, *8*, 67−77.
(30) Quan, F.-S.; Rubino, I.; Lee, S.-H.; Koch, B.; Choi, H.-J. Universal and Reusable Virus Deactivation System for Respiratory Protection. *Sci. Rep.* **2017**, *7*, 39956.
(31) Xiong, R.; Hua, D.; van Hoeck, J.; Berdecka, D.; Léger, L.; de Munter, S.; Fraire, J. C.; Raes, L.; Harizaj, A.; Sauvage, F.; Goetgeluk, G.; Pille, M.; Aalders, J.; Belza, J.; van Acker, T.; Bolea-Fernandez, E.; Si, T.; Vanhaecke, F.; de Vos, W. H.; Vandekerckhove, B.; van Hengel, J.; Raemdonck, K.; Huang, C.; de Smedt, S. C.; Braeckmans, K. Photothermal Nanofibres Enable Safe Engineering of Therapeutic Cells. *Nat. Nanotechnol.* **2021**, *16*, 1281−1291.
(32) Madni, A.; Kousar, R.; Naeem, N.; Wahid, F. Recent Advancements in Applications of Chitosan-Based Biomaterials for Skin Tissue Engineering. *J. Bioresour. Bioprod.* **2021**, *6*, 11−25.
(33) Arora, A.; Mishra, A. Antibacterial Polymers − A Mini Review. *Mater. Today: Proc.* **2018**, *5*, 17156−17161.
(34) Ding, X.; Duan, S.; Ding, S.; Liu, R.; Xu, F.-J. Versatile Antibacterial Materials: An Emerging Arsenal for Combatting Bacterial Pathogens. *Adv. Funct. Mater.* **2018**, *28*, No. 180214.
(35) Liu, H.; Elkin, I.; Chen, J.; Klibanov, A. M. Why Do Some Immobilized N-Alkylated Polyethylenimines Far Surpass Others in Inactivating Influenza Viruses? *Biomacromolecules* **2015**, *16*, 351−356.
(36) Larson, A. M.; Oh, H. S.; Knipe, D. M.; Klibanov, A. M. Decreasing Herpes Simplex Viral Infectivity in Solution by Surface-Immobilized and Suspended *N*,*N*-dodecyl,methyl-Polyethylenimine. *Pharm. Res.* **2013**, *30*, 25−31.
(37) Tiliket, G.; Sage, D. L.; Moules, V.; Rosa-Calatrava, M.; Lina, B.; Valleton, J. M.; Nguyen, Q. T.; Lebrun, L. A New Material for Airborne Virus Filtration. *Chem. Eng. J.* **2011**, *173*, 341−351.
(38) Haldar, J.; An, D.; Álvarez de Cienfuegos, L.; Chen, J.; Klibanov, A. M. Polymeric Coatings that Inactivate Both Influenza Virus and Pathogenic Bacteria. *Proc. Natl. Acad. Sci. U. S. A.* **2006**, *103*, 17667−17671.
(39) Haldar, J.; Chen, J.; Tumpey, T. M.; Gubareva, L. V.; Klibanov, A. M. Hydrophobic Polycationic Coatings Inactivate Wild-Type and Zanamivir-and/or Oseltamivir-Resistant Human and Avian Influenza Viruses. *Biotechnol. Lett.* **2008**, *30*, 475−479.
(40) Larson, A. M.; Hsu, B. B.; Rautaray, D.; Haldar, J.; Chen, J.; Klibanov, A. M. Hydrophobic Polycationic Coatings Disinfect Poliovirus and Rotavirus Solutions. *Biotechnol. Bioeng.* **2011**, *108*, 720−723.

https://doi.org/10.1021/acsami.2c04165
ACS Appl. Mater. Interfaces 2022, 14, 25135−25146

(41) Tuladhar, E.; de Koning, M. C.; Fundeanu, I.; Beumer, R.; Duizer, E. Different Virucidal Activities of Hyperbranched Quaternary Ammonium Coatings on Poliovirus and Influenza Virus. *Appl. Environ. Microbiol.* **2012**, *78*, 2456−2458.
(42) Tsao, I.-F.; Wang, H. Y.; Shipman, C. Interaction of Infectious Viral Particles with a Quaternary Ammonium Chloride (QAC) Surface. *Biotechnol. Bioeng.* **1989**, *34*, 639−646.
(43) Kumaran, S.; Oh, E.; Han, S.; Choi, H.-J. Photopolymerizable, Universal Antimicrobial Coating to Produce High-Performing, Multifunctional Face Masks. *Nano Lett.* **2021**, *21*, 5422−5429.
(44) Ren, T.; Dormitorio, T. V.; Qiao, M.; Huang, T.-S.; Weese, J. N-Halamine Incorporated Antimicrobial Nonwoven Fabrics for Use Against Avian Influenza Virus. *Vet. Microbiol.* **2018**, *218*, 78−83.
(45) He, X.; Xing, R.; Liu, S.; Qin, Y.; Li, K.; Yu, H.; Li, P. The Improved Antiviral Activities of Amino-Modified Chitosan Derivatives on Newcastle Virus. *Drug Chem. Toxicol.* **2021**, *44*, 335−340.
(46) Catel-Ferreira, M.; Tnani, H.; Hellio, C.; Cosette, P.; Lebrun, L. Antiviral Effects of Polyphenols: Development of Bio-Based Cleaning Wipes and Filters. *J. Virol. Methods* **2015**, *212*, 1−7.
(47) Monge, F. A.; Jagadesan, P.; Bondu, V.; Donabedian, P. L.; Ista, L.; Chi, E. Y.; Schanze, K. S.; Whitten, D. G.; Kell, A. M. Highly Effective Inactivation of SARS-Cov-2 By Conjugated Polymers and Oligomers. *ACS Appl. Mater. Interfaces* **2020**, *12*, 55688−55695.
(48) Dhende, V. P.; Samanta, S.; Jones, D. M.; Hardin, I. R.; Locklin, J. One-Step Photochemical Synthesis of Permanent, Nonleaching, Ultrathin Antimicrobial Coatings for Textiles and Plastics. *ACS Appl. Mater. Interfaces* **2011**, *3*, 2830−2837.
(49) Public Health Service, Department of Health and Human Services. *Title 42 Chapter I Subchapter G Part 84 − Approval of Respiratory Protective Devices Subpart K − Non-Powered Air-Purifying Particulate Respirators (42CFR84.181)*. Govinfo.gov October 1, 2009. Accessed 20 January 2022.
(50) Beattie, J. K. The Intrinsic Charge on Hydrophobic Microfluidic Substrates. *Lab Chip* **2006**, *6*, 1409−1411.
(51) Zangi, R.; Engberts, J. B. F. N. Physisorption of Hydroxide Ions from Aqueous Solution to a Hydrophobic Surface. *J. Am. Chem. Soc.* **2005**, *127*, 2272−2276.
(52) Ngankam, A. P.; van Tassel, P. R. Continuous Polyelectrolyte Adsorption Under an Applied Electric Potential. *Proc. Natl. Acad. Sci. U. S. A.* **2007**, *104*, 1140−1145.
(53) de Vos, W. M.; Lindhoud, S. Overcharging and Charge Inversion: Finding the Correct Explanation(s). *Adv. Colloid Interface Sci.* **2019**, *274*, No. 102040.
(54) Latour, R. A. Fundamental Principles of The Thermodynamics and Kinetics of Protein Adsorption to Material Surfaces. *Colloids Surf. B Biointerfaces* **2020**, *191*, No. 110992.
(55) U.S. Consumer Product Safety Commission. *Part 1610—Standard for the Flammability of Clothing Textiles: Subpart A 1610.4 Requirements for Classifying Textiles (16CFR1610.4)*. Govinfo.gov January 1, 2016. Accessed 20 January 2022.
(56) Food and Drug Administration, Department of Health and Human Services. *Title 21 Chapter 1 Subchapter H part 878 General and Plastic Surgery Devices Subpart E Surgical Devices (21CFR878.4040-Surgical Apparel)*. Govinfo.gov April 1, 2004. Accessed 20 January 2022
(57) Cui, J.; Wang, Y.; Lu, T.; Liu, K.; Huang, C. High Performance, Environmentally Friendly and Sustainable Nanofiber Membrane Filter for Removal of Particulate Matter 1.0. *J. Colloid Interface Sci.* **2021**, *597*, 48−55.
(58) Xiao, H.; Song, Y.; Chen, G. Correlation Between Charge Decay and Solvent Effect for Melt-Blown Polypropylene Electret Filter Fabrics. *J. Electrostat.* **2014**, *72*, 311−314.
(59) Gao, J.; Huddleston, N. E.; White, E. M.; Pant, J.; Handa, H.; Locklin, J. Surface Grafted Antimicrobial Polymer Networks with High Abrasion Resistance. *ACS Biomater. Sci. Eng.* **2016**, *2*, 1169−1179.
(60) Ergene, C.; Yasuhara, K.; Palermo, E. F. Biomimetic Antimicrobial Polymers: Recent Advances in Molecular Design. *Polym. Chem.* **2018**, *9*, 2407−2427.
(61) Konai, M. M.; Bhattacharjee, B.; Ghosh, S.; Haldar, J. Recent Progress in Polymer Research to Tackle Infections and Antimicrobial Resistance. *Biomacromolecules* **2018**, *19*, 1888−1917.
(62) Rakowska, P. D.; Tiddia, M.; Faruqui, N.; Bankier, C.; Pei, Y.; Pollard, A. J.; Zhang, J.; Gilmore, I. S. Antiviral Surfaces and Coatings and Their Mechanisms of Action. *Commun. Mater.* **2021**, *2*, 53.
(63) Palermo, E. F.; Kuroda, K. Chemical Structure of Cationic Groups in Amphiphilic Polymethacrylates Modulates the Antimicrobial and Hemolytic Activities. *Biomacromolecules* **2009**, *10*, 1416−1428.
(64) Joshi, P. U.; Meingast, C. L.; Xu, X.; Holstein, M.; Feroz, H.; Ranjan, S.; Ghose, S.; Li, Z. J.; Heldt, C. L. Virus Inactivation at Moderately Low pH Varies with Virus and Buffer Properties. *Biotechnol. J.* **2022**, *17*, No. 2100320.
(65) Körner, R. W.; Majjouti, M.; Alcazar, M.; Mahabir, E. Of Mice and Men: The Coronavirus MHV and Mouse Models as a Translational Approach to Understand SARS-CoV-2. *Viruses* **2020**, *12*, 880.
(66) Heldt, C. L.; Hernandez, R.; Mudiganti, U.; Gurgel, P. V.; Brown, D. T.; Carbonell, R. G. A Colorimetric Assay for Viral Agents that Produce Cytopathic Effects. *J. Virol. Methods* **2006**, *135*, 56−65.
(67) Benskey, M.J.; Manfredsson, F. P. Lentivirus Production and Purification. In *Gene Therapy for Neurological Disorders: Methods and Protocols (Methods in Molecular Biology #1382)*; Humana Press, 2016, 107−114.
(68) Meingast, C.; Joshi, P. U.; Turpeinen, D. G.; Xu, X.; Holstein, M.; Feroz, H.; Ranjan, S.; Ghose, S.; Li, Z. J.; Heldt, C. L. Physiochemical Properties of Enveloped Viruses and Arginine Dictate Inactivation. *Biotechnol. J.* **2021**, *16*, No. e2000342.
(69) Allison, B. C.; Applegate, B. M.; Youngblood, J. P. Hemocompatibility of Hydrophilic Antimicrobial Copolymers of Alkylated 4-Vinylpyridine. *Biomacromolecules* **2007**, *8*, 2995−2999.
(70) Lei, C.; Yang, J.; Hu, J.; Sun, X. On the Calculation of TCID50 for Quantitation of Virus Infectivity. *Virol. Sin.* **2021**, *36*, 141−144.
(71) Rockey, N.; Arts, P. J.; Li, L.; Harrison, K. R.; Langenfeld, K.; Fitzsimmons, W. J.; Lauring, A. S.; Love, N. G.; Kaye, K. S.; Raskin, L.; Roberts, W. W.; Hegarty, B.; Wigginton, K. R. Humidity and Deposition Solution Play a Critical Role in Virus Inactivation by Heat Treatment of N95 Respirators. *mSphere* **2020**, *5*, e00588−e00520.

https://doi.org/10.1021/acsami.2c04165
ACS Appl. Mater. Interfaces 2022, 14, 25135−25146